Journal of Solid State Chemistry 184 (2011) 2516–2524

Contents lists available at ScienceDirect

Journal of Solid State Chemistry

journal homepage: www.elsevier.com/locate/jssc

Local deuterium order in apparently disordered Laves phase deuteride $YFe_2D_{4.2}$

J. Ropka [a], R. Černý [a,*], V. Paul-Boncour [b]

[a] Laboratory of Crystallography, University of Geneva, Quai E.-Ansermet 24, CH-1211 Geneva, Switzerland
[b] CMTR, ICMPE, CNRS, 2 rue H. Dunant, 94320 Thiais Cedex, France

ARTICLE INFO

Article history:
Received 9 March 2011
Received in revised form
14 July 2011
Accepted 17 July 2011
Available online 26 July 2011

Keywords:
Metal hydride
Local order
Pair Distribution Function
Neutron powder diffraction

ABSTRACT

Deuterium short-range order in cubic Laves phase deuteride $YFe_2D_{4.2}$ was studied by neutron (*ToF*) powder diffraction experiments and Pair Distribution Function (PDF) analysis between 290 and 400 K. The minimal allowed D–D distance of 2.1 Å in a metal deuteride (Switendick rule) has been experimentally proved in the HT-disordered phase $YFe_2D_{4.2}$. It has been found that the distribution of deuterium atoms around the iron is not random, and cannot be explained only by applying the Switendick rule. The first coordination sphere of iron atoms in the high temperature (HT)-disordered phase resembles between 350 and 400 K the coordination observed in the low temperature (LT)-ordered phase. Reversed Monte Carlo modeling of the Pair Distribution Function of the HT-disordered phase prefers the coordination FeD_5 and FeD_4 in agreement with the LT-ordered phase.

1. Introduction

The deuterides of cubic (C15) Laves phases AB_2 (*A*-rare earth, *B*-transition metal) have been widely studied for the influence of deuterium absorption on their magnetic properties. YFe_2, which can absorb up to 5H per formula unit (/f.u.), is particularly interesting owing to the large variety of crystal structures obtained at different hydrogen content [1–8]. These crystal structures are related to an ordering of hydrogen atoms on interstitial sites below an order–disorder temperature T_{OD}, which leads either to superstructures or to a distortion of the cubic C15 structure. The deuterium rich phase $YFe_2D_{4.2}$ shows complex magnetic and structural behavior and was object of numerous studies [7–10].

1.1. Structural models of HT-disordered and LT-ordered $YFe_2D_{4.2}$ phases

Above $T_{OD}=338$ K, $YFe_2D_{4.2}$ crystallizes in the cubic structure (*Fd*-3*m*, $a=7.95$ Å); between 332 and 338 K it shows a rhombohedral distortion (*R*-3*m*, $a=5.702$ Å, $c=12.404$ Å) [7]; and below 332 K it has a monoclinic superstructure (*Pc*, $a=5.5066$, $b=11.4823$, $c=9.4292$ Å, $\beta=122.33^\circ$ at 290 K) [9,10].

The LT-ordered monoclinic $YFe_2D_{4.2}$ contains seven of eight independent iron atoms coordinated by deuterium in a trigonal bipyramid. The eighth iron atom (Fe8) is coordinated by four deuterium in a tetrahedral configuration. Most D–D distances are, within the precision of the diffraction experiment, longer than 2.1 Å; the shortest ones are of 1.96 Å. Among 64 available sites (48 sites A_2B_2 and 16 sites AB_3) 18 sites (15 sites A_2B_2 and 3 sites AB_3) were occupied by deuterium, from which 10 sites not fully (occupancy between 0.835 and 0.974). The notation A_2B_2 and AB_3 of the deuterium sites refers to the tetrahedral coordination of the sites by the metals. The refined composition of the LT-ordered phase is therefore $YFe_2D_{4.27(5)}$ in agreement with the D content obtained by the volumetric method. See Ref. [10] for more details and for structural drawings.

The structural model of the HT-disordered cubic phase as seen by the Rietveld refinement is shown in Fig. 1. Deuterium atoms are distributed on two Wyckoff sites, 96*g* and 32*e*, with tetrahedral coordination by metals (A_2B_2 and AB_3, resp.) with a strong preference for the 96*g* site and third available tetrahedral site 8*b* (B_4) empty (see Supporting Information, Table S1, Fig. S1 and Ref. [10]). The total number of deuterium atoms in one cubic unit cell of the HT-disordered phase is 34 if calculated from the refined composition of the LT-ordered phase, and 37 as refined for the HT-disordered phase. This discrepancy was discussed in [10] in view of not exact treatment of the diffuse intensity in the neutron powder pattern of the HT-disordered phase by Rietveld refinement. In our next analysis of the HT-disordered phase we will introduce 34 deuterium atoms/cubic unit cell. Our choice to work with 34 instead of 37 atoms is based on the observation that the order–disorder transition between the LT- and HT-phases is fully reversible, and the Rietveld refinement of the ordered LT-phase is

* Corresponding author.
E-mail address: Radovan.Cerny@unige.ch (R. Černý).

0022-4596/$ - see front matter © 2011 Elsevier Inc. All rights reserved.
doi:10.1016/j.jssc.2011.07.028

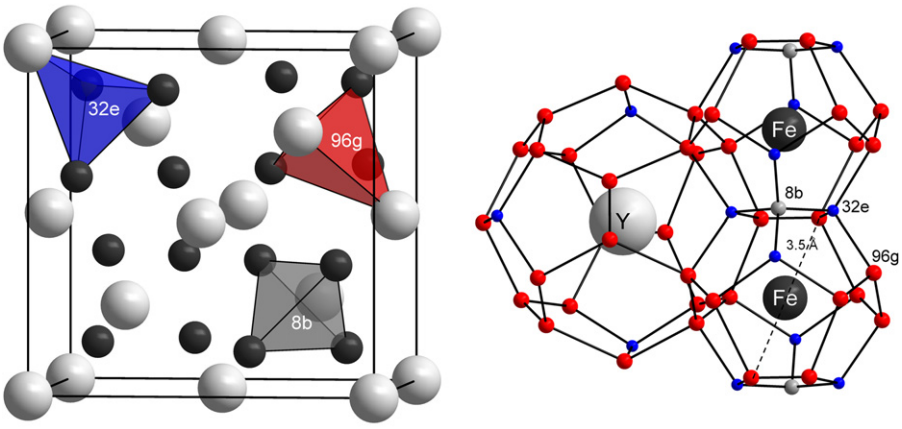

Fig. 1. Structural model of the HT-disordered phase as seen by the Rietveld refinement. Left: one cubic unit cell, yttrium as light and iron as dark spheres. Deuterium atoms are distributed on two Wyckoff sites, 96*g* and 32*e*, with tetrahedral coordination by metals (A_2B_2 and AB_3, respectively) with a strong preference for the 96*g* site and third available tetrahedral site 8*b* (B_4) empty. Right: coordination of yttrium and iron atoms by the deuterium. The maximal distance of 3.5 Å between two deuterium atoms in the first coordination sphere of the iron is shown by a dashed line.

more reliable as the powder pattern contains only Bragg contribution and no diffuse intensity.

The order–disorder transitions very often include a short-range order (SRO) in the disordered phase as a precursor to an ordering phase transition inducing the long-range order (LRO). A classic example is the ordering of deuterium atoms in deuterides of *bcc* metals like $VD_{0.8}$ [11] or $PdD_{0.5}$ [12]. The question whether the SRO exists also in the HT-$YFe_2D_{4.2}$ cannot be answered from the analysis of Bragg scattering, therefore the diffuse intensity in the neutron scattering data must be analyzed. Indeed the diffuse intensity was observed in the neutron powder patterns of HT-$YFe_2D_{4.2}$ [10]. The SRO of deuterium atoms in HT-disordered cubic Laves phases was observed and explained for HfV_2D_4 [13], ZrV_2D_4 [14] and for $ZrCr_2D_4$ [15]. It was found that the dominating contribution to the neutron diffuse scattering comes from the chemical SRO between deuterium atoms and vacancies on 96*g* and 32*e* Wyckoff sites. In $ZrCr_2D_4$ also the displacive SRO was modeled. No D–D distances shorter than 2.1 Å have been observed, strong D–D correlations up to 4 Å, and no D–D correlations (random D distribution) above 12 Å have been concluded from the Reversed Monte Carlo modeling in the reciprocal space.

In this paper we will show that the SRO also exists in the HT-$YFe_2D_{4.2}$, and we will compare it to the LRO as observed in the LT-$YFe_2D_{4.2}$. As the experimental method we will use the Pair Distribution Function analysis of the diffuse intensity in the neutron powder pattern.

2. Experimental

2.1. Sample synthesis and DSC measurement

The YFe_2 intermetallic compound was prepared by induction melting of the pure elements followed by 3 weeks of annealing at 1100 K. The composition and homogeneity was checked by X-ray powder diffraction (XPD) using a Bruker D8 diffractometer (Cu $K\alpha$ radiation) and electron probe microanalysis (EPMA) as described in [7]. The $YFe_2D_{4.2}$ deuteride was prepared by solid-gas reaction using a Sievert apparatus as described in [7], and its homogeneity was checked by XPD. The sample used for the PDF analysis in this paper corresponds to the sample no. 1 from the Ref. [10].

The thermal behavior of the order–disorder transition was measured using a differential scanning calorimeter DSC Q100 from TA instrument, with heating rate of 5 and 10 K/min.

2.2. Pair Distribution Function analysis

The analysis of the Bragg scattering assumes a LRO in the crystal, and is done for polycrystalline samples via Rietveld refinement [16]. Deviations from the LRO result in the occurrence of diffuse scattering which contains information about SRO of atoms. In a total scattering experiment which samples Bragg and diffuse scattering data simultaneously the information about SRO is preserved. There are various ways to extract information about the SRO from the analysis of single crystal diffuse scattering [17]. Significant, and often sufficient, information can be gleaned from the analysis of the atomic Pair Distribution Function (PDF) obtained from the total scattering from powder samples, and experiment as well as data analysis are in general less complicated. In fact the PDF method was originally applied to the study of liquids and amorphous materials [18], but can also be applied to disordered crystalline materials [19].

The PDF gives the volume normalized probability of finding an atom at a given distance r from another atom. In other words it can be understood as a bond length distribution of the material weighted by the respective scattering powers of the contributing atoms. The PDF can be calculated from a structural model, according to the definition of $\rho(r)$ from [20], by a relation

$$G_{calc}(r) = \frac{1}{r}\sum_{ij}\left[\frac{b_i b_j}{\langle b\rangle^2}\delta(r-r_{ij})\right] - 4\pi r\rho_0 \quad (1)$$

where ρ_0 is the average number density. The sum goes over all pairs of atoms i and j within the model crystal separated by r_{ij} [19]. The scattering power of atom i is b_i and $<b>$ is the average scattering power of the sample. In the case of neutron scattering b_i is simply the scattering length of the atom i.

The observed PDF is obtained [21,22] from the powder diffraction data via a *sine* Fourier transform of the normalized total-scattering structure function $S(Q)$

$$G_{obs}(r) = 4\pi r[\rho(r)-\rho_0] = \frac{2}{\pi}\int_0^\infty Q[S(Q)-1]\sin(Qr)dQ \quad (2)$$

where $\rho(r)$ is the microscopic pair density.

2.3. Time-of-flight neutron data

The time-of-flight (*ToF*) neutron powder data were collected at the GPPD diffractometer at the IPNS, Argonne National Laboratory

(T=290, 350 and 400 K). The sample (7.7 g of fine powder) was closed in a vanadium container, and the temperature was controlled by the Displex attachment. The empty vanadium container mounted on the Displex attachment was also measured allowing us to assess and subtract instrumental background. The scattering from a vanadium rod was also measured allowing the data to be normalized for the incident spectrum and detector efficiencies. All data were measured from the magnitude of the scattering vector $Q(=4\pi \sin\theta/\lambda)$ of $\sim$1 up to 30 Å^{-1}. The raw data were corrected for absorption, multiple scattering, and inelastic scattering (Placzek correction) using the procedures implemented in the program *PDFgetN* [23].

The paramagnetic scattering of iron atoms in both $YFe_2D_{4.2}$ phases was neglected. Indeed the magnetic moment of the iron is about 1 Bohr magnetron above the magnetic ordering temperature of 131 K, and continues to decrease with increasing temperature [7]. The magnetic scattering length $b_{magnetic}$ of 1 Bohr magnetron is 0.27 fm, while the average nuclear scattering length $b_{nuclear}$ of $YFe_2D_{4.2}$ is 7.59 fm, so that $[b_{magnetic}/b_{nuclear}]^2=0.00126$. The magnetic peak intensity will be only 0.126% of the nuclear peak intensity, completely negligible in the observed PDFs.

After being corrected the data are normalized by the total scattering cross-section of the sample to yield the total scattering structure function $S(Q)$, and the observed PDF is obtain via the Eq. (2).

2.4. Analysis and modeling of PDF

The observed PDFs were compared to the PDFs calculated from structural models of monoclinic LT-ordered and cubic HT-disordered $YFe_2D_{4.2}$ phases obtained by Rietveld refinement of the *ToF* data [10]. The program *PDFgui* [24] was used for calculating the PDF from a structural model, and for the least-square fitting to the observed PDF. The thermal motion and static displacements of the atoms from average positions as obtained from the Rietveld refinement have been modeled as PDF peak broadening which does not depend on r for uncorrelated mean-square thermal displacements, and is r-dependent for the correlated motion which is at the origin of thermal diffuse scattering. The form of the r-dependency for the correlated motion broadening is given in Ref. [25]. Only the term varying as $1/r^2$ corresponding to the temperatures higher than Debye temperature of the studied material was used. The atomic positions, isotropic displacement parameters and site occupancy factors were fixed to the values from Rietveld refinement [10]. Only lattice parameters, scale factor and r-dependent PDF peak broadening parameters were allowed to vary. The lattice parameters have been varied, because their values obtained from the PDF analyses can differ from those obtained from Rietveld refinement due to different treatment of the instrumental resolution function in both analyses; see e.g. [26]. The minimal interatomic distance r used in the refinement or modeling of the observed PDFs was 0.95 Å as the shorter r-range contains too strong oscillations due to the termination error in the Fourier transformation [19].

The modeling of the PDF observed from the HT-disordered phase was then done by Reverse Monte Carlo (RMC) method as available in the program *DISCUS* [27]. As a starting point for the *RMC modeling* we have used a random distribution of 34 deuterium atoms on 136 positions of the three Wyckoff sites (96*g*, 32*e* and 8*b*) of one cubic unit cell. A periodic refinement box of local symmetry has to be chosen for the RMC modeling, which is at least two times bigger than the investigated correlation length [19]. As we study the correlations up to $\sim$8 Å (see later), a cube of the size $\sim$16 Å, i.e. 8 cubic unit cells of the HT-$YFe_2D_{4.2}$ has been selected as the refinement box. Only the chemistry swaps between a deuterium atom and a vacancy were allowed as the Monte Carlo moves. The displacive moves (shifts of atoms from the average positions) have not been considered, contrary to the Ref. [15]. This is because no evidence for disorder on atomic positions has been observed in the values of displacement parameters from the Rietveld refinement [10]. No constraints of a minimal distance between two deuterium atoms were used in the modeling with one exception explained later. The observed PDF was fitted by the *RMC modeling* in two r-ranges: 0.95–3.8 Å called *short-range RMC model*, and 3.8–8.0 Å called *long-range RMC model*. The atomic positions and isotropic displacement parameters were fixed to the values from Rietveld refinement, and r-dependent PDF peak broadening parameters to the values obtained from the *PDFgui* fitting. Around 100 independent RMC runs were repeated for each modeling in the view of obtaining good statistics of the results. The annealing temperature, as defined in *DISCUS*, was 0.04 which corresponds to the ratio of accepted RMC steps good/bad as 3/1 (see Supporting Information, Fig. S2 and Table S2). The agreement between the calculated and observed PDF was described using the agreement factor R_{wp} (equivalent to the R_{wp} from the Rietveld refinement) calculated by *PDFgui* as

$$R_{wp}=\sqrt{\frac{\sum_{i=1}^{N} w(r_i)[G_{obs}(r_i)-G_{calc}(r_i)]^2}{\sum_{i=1}^{N} w(r_i)G_{obs}^2(r_i)}} \quad (3)$$

where the weights $w(r_i)$ are obtained from the observed PDF, and the summation goes over N data points used in the refinement r-range.

3. Results and discussion

3.1. Phase transition order–disorder

The DSC measurements (Fig. 2) shows two peaks centered at 332 and 338 K upon heating which can be attributed to the two structural transitions induced by deuterium ordering on particular tetrahedral interstitial sites. The enthalpies of the transitions are 4.5 and 0.25 J/g, resp. According to [7], the peak at 332 K corresponds to the transition between monoclinic and rhombohedral phase, and the peak at 338 K to the transition between rhombohedral and cubic structures.

3.2. PDF from LT-ordered and HT-disordered phases

Powder patterns from medium resolution GPPD data bank for LT-ordered and HT-disordered $YFe_2D_{4.2}$ phases are shown in Fig. 3. Note that the diffuse intensity in the HT-disordered

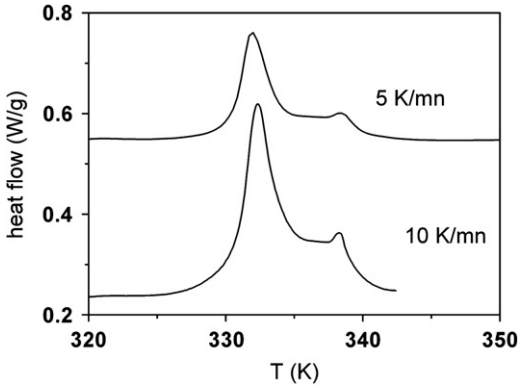

Fig. 2. DSC curves with heating rate of 5 and 10 K/min, respectively, showing two order–disorder phase transitions in $YFe_2D_{4.2}$: between monoclinic and rhombohedral phase at 332 K, and between rhombohedral and cubic phase at 338 K.

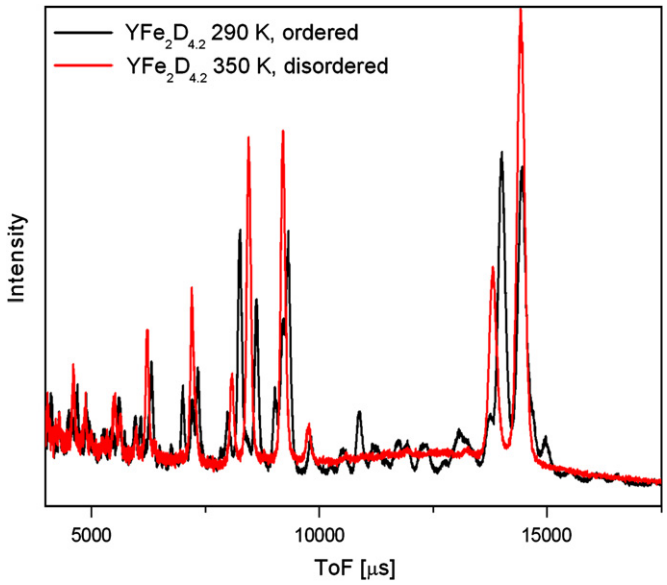

Fig. 3. Part of the neutron powder pattern (intensity *vs.* time-of-flight) from medium resolution GPPD data bank for LT-ordered (290 K) and HT-disordered (350 K) $YFe_2D_{4.2}$. Note the diffuse intensity in the HT-disordered phase in the same *ToF*-region where the superstructure reflections appear in the LT-ordered phase.

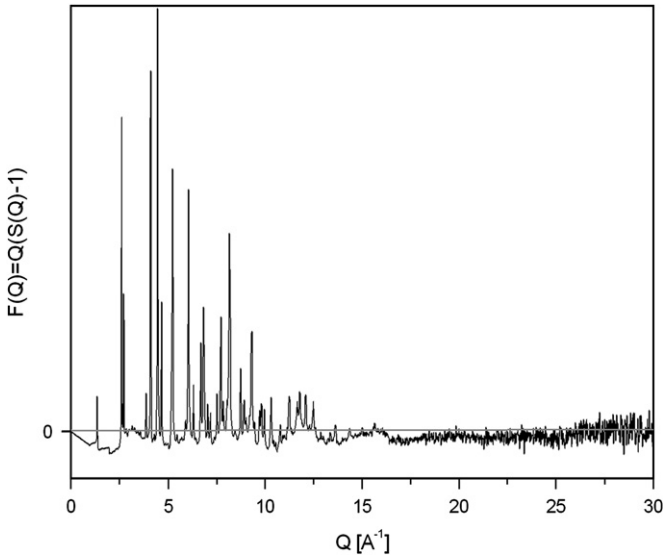

Fig. 4. Normalized total-scattering structure function $S(Q)$ of the HT-disordered $YFe_2D_{4.2}$ phase at 350 K as obtained from the GPPD data.

phase is located in the same *ToF* region where the superstructure reflections appear in the LT-ordered phase. Normalized total-scattering structure function $S(Q)$ of the HT-disordered phase at 350 K as obtained from the GPPD data is shown in Fig. 4.

Upon inspection of the observed PDFs of LT-ordered (290 K) and HT-disordered (350 K) $YFe_2D_{4.2}$ phases given in Fig. 5, one will immediately notice the similarity of both PDFs up to $r\sim3.8$ Å, and even up to ~8 Å. The r-range up to 3.8 Å has been selected as a range of interest as it includes all atomic pair interactions within the first coordination sphere of iron atoms as it is shown in Fig. 1. The similarity of both observed PDFs can be understood as the similarity of the local structures of LT-ordered and HT-disordered phases up to this correlation length, at least within the radial projection onto the PDF. In contrast to the SRO, the LRO in both phases is quite different as it follows from the increasing

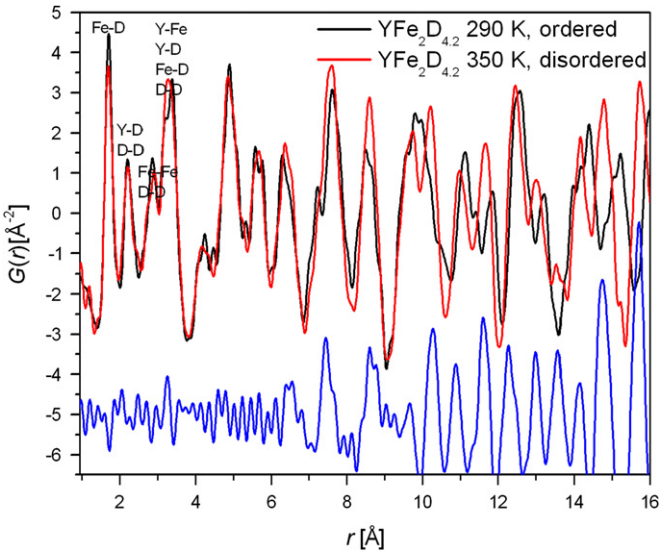

Fig. 5. Observed PDFs from the LT-ordered (290 K) and HT-disordered (350 K) $YFe_2D_{4.2}$. The difference curve is shown below. First four peaks are labeled according to the known crystal structures from Rietveld refinement.

difference between both PDFs above $r\sim8$ Å. The same conclusion about the similarity of SRO on LT-ordered and HT-disordered Laves phase deuterides has been done already for $ZrCr_2D_4$ in the Ref. [15]. The similarity of the PDFs for LT- and HT-$YFe_2D_{4.2}$ in the range up to $r\sim3.8$ Å does not change with the temperature up to 400 K (see Supporting Information, Fig. S3). This means that the SRO in the HT-phase reflects rather strong interatomic interactions like Fe–D bonding which evolutes only slightly with the temperature up to 400 K. The deuterium desorption from the HT-$YFe_2D_{4.2}$ starts above 400 K [28].

The second observation one can deduce from Fig. 5 is the absence of any D–D interatomic distances shorter than 2.1 Å in both PDFs whereas Fe–D distances of ~1.7 Å are observed as attributed from the refined structure of the LT-ordered phase. It confirms the usual observation, known as Switendick rule [29] that in fully ordered metal deuterides the minimal distance between two deuterium atoms is longer than 2.1 Å due to repulsive D–D interactions. This observation is not surprising for the LT-ordered phase, as it is already available from the Bragg intensities. On the contrary no such conclusion was possible to do from the Rietveld refinement of the HT-disordered deuteride, and can be done only from the analysis of diffuse scattering.

The third observation is that the first peak at $r\sim1.7$ Å corresponding to the first coordination sphere Fe–D is clearly narrower in both PDFs than peaks at higher r-values. The Fe–D distances as refined by the Rietveld method using the *ToF* data of the LT-ordered phase are distributed within the range 1.618(7)–1.875(8) Å [10] with the maximum around 1.7 Å, in agreement with the first PDF peak. This peak is nearly identical in PDFs of LT- and HT-phases, with the exception of a slight peak broadening at higher temperature due to the thermal vibrations. The narrow first PDF peak can be understood as a correlated thermal motion or static displacement of quite rigid coordination polyhedra FeD_x in both, LT-ordered and HT-disordered phases. Attribution of further PDF peaks to known interatomic distances becomes difficult as there is an increasing number of interatomic distances which start to overlap in a cluster of PDF peaks as all three atomic species, iron, yttrium and deuterium are quite strong neutron scatterers. The most important contributions as derived from the Rietveld refinement are labeled in Fig. 5 up to $r\sim3.8$ Å.

The observed PDFs were then compared to the PDFs calculated from the structural models of monoclinic LT-ordered and cubic HT-disordered $YFe_2D_{4.2}$ phases obtained from the Rietveld refinement. The Rietveld plots for the HT-disordered phase are given in the Supporting Information as Fig. S1, and the Rietveld plots for the LT-ordered phase can be consulted in the Ref. [10] where also more details about the refinement can be found.

As a reference for the accuracy of our next PDF modeling we show the observed PDF of the LT-ordered phase compared with the PDF calculated from the ordered monoclinic structure [10] as obtained from the Rietveld refinement (Supporting Information, Fig. S4). The agreement factor R_{wp} was within 0.19–0.20 for all r-ranges (Table 1) showing no neglected local correlations in the Rietveld model of the LT-ordered phase. The notation of Wyckoff sites identified in the monoclinic structure as A_2B_2 and AB_3 sites corresponds to the cubic HT-disordered phase.

Then we compare the PDFs of HT-disordered $YFe_2D_{4.2}$ as observed and as calculated from the *Rietveld model*, i.e. model with the deuterium occupying all 136 atomic sites in a unit cell with occupancies according to the Rietveld refinement (Fig. 6 top). The agreement factors R_{wp} for different r-ranges are given in Table 1. Clearly the agreement is quite bad in the r-range 0.95–3.8 Å, the first coordination sphere of iron.

3.3. Random (Switendick) model of deuterium distribution in the HT-disordered phase

Next we calculate the PDF from a *random distribution* of 34 deuterium atoms on 136 available atomic positions with the only constraint of a minimal distance between two deuterium atoms of 1.96 Å. Shorter minimal distance than Switendick rule was chosen, because in the LT-ordered phase the shortest D–D distances are of 1.96 Å. The *Switendick model* has been created as follows.

One possible deuterium position was randomly selected among all available positions, and its neighborhood was checked. If there were no other deuterium atoms 1.96 Å apart, the deuterium was placed on this randomly selected position. This procedure was repeated as long as all deuterium atoms (34) were successfully placed. In total more than 500 crystals were independently created by this algorithm. There are 16 iron atoms in each crystal. It gives 8000 iron probes in total. From the analysis of these 8000 probes it follows that the coordination number varies between 2 and 8 (it will be discussed later). The distribution of deuterium atoms between the three Wyckoff sites calculated as an average from all 500 crystals differs from the *Rietveld model* as it can be seen in Table 1. Especially the 8*b* site refined by the Rietveld refinement and also observed in the LT-ordered phase as nearly empty, has 50% occupancy in the *Switendick model*!

The PDFs have been calculated from several crystals of the *Switendick model*, and compared to the observed PDF of the HT-disordered phase. Results of one representative crystal are shown in Fig. 6 bottom. One can again clearly see that the *Switendick model* does not explain well the observed PDF in the region up to ~3.8 Å, which includes the maximal D–D distance found within the first coordination sphere of the iron (see Fig. 1 right). The disagreement decreases with increasing r, but increases again for the range 8.0–16 Å. As the *Switendick model* is not a result of any modeling of the scattering data, but of a strict application of the Switendick rule only, the only conclusion that can be obtained from the behavior of the agreement factor R_{wp} is that the Switendick rule itself does not explain the distribution of deuterium atoms within the first coordination sphere of iron.

3.4. Reverse Monte Carlo modeling of deuterium distribution in the HT-disordered phase

As the R_{wp} of the *Rietveld model* for the r-range 0.95–3.8 is significantly higher than for ranges above 3.8 Å, we can conclude that the distribution of deuterium atoms in the first coordination spheres of iron and yttrium atoms is not random, as observed by the Rietveld refinement, but follows a SRO. The next step was to find a model of the local order which can explain the observed PDF. It has been done by using the *RMC modeling* and two, "*short-range*" (0.95–3.8 Å) and "*long-range*" (3.8–8.0 Å), *RMC models*. The agreement factors R_{wp} calculated for different r-ranges of both RMC modeling are given in Table 1. A comparison of the observed PDF for the HT-disordered phase with the PDF calculated from the *short-range RMC model* is shown in Fig. 7 top, and from the *long-range RMC model* in Fig. 7 middle.

Compared to the *Rietveld model*, the *RMC modeling* improves the agreement of the observed and calculated PDFs significantly in the range 0.95–3.8 Å when the fitting is done within this range (*short-range RMC model*). When the fitting is done within the range 3.8–8.0 Å (*long-range RMC model*), the agreement in the range 0.95–3.8 Å is much worse. On the other hand the agreement of the observed and calculated PDFs in the ranges above 3.8 Å is only slightly improved by the *short-range RMC model*, but

Table 1
Agreement factors R_{wp} calculated for different r-ranges and for different models of the HT-disordered phase $YFe_2D_{4.2}$. The *long-range RMC model* corresponds to modeling within $r=3.8-8.0$ Å, the *short-range RMC model* corresponds to modeling within $r=0.95-3.8$ Å. In the first column also the values for the LT-ordered phase are shown as a reference (the notation of Wyckoff sites identified in the monoclinic LT-ordered phase as A_2B_2 and AB_3 sites corresponds to the cubic HT-disordered phase).

Agreement factors R_{wp}							
	LT-ordered phase	*HT-disordered phase*					
r-Range	*Rietveld model*	*LT-ordered model*	*Rietveld model*	*Switendick model*	*Long-range RMC model* (16 Å *box*)	*Short-range RMC model* (16 Å *box*)	*Short-range RMC+Switendick model* (8 Å *box*)
0.95–3.8 Å	0.19	0.25	0.37	0.35	0.42	0.22	0.23
3.8–8.0 Å	0.20	0.19	0.25	0.25	0.13	0.18	0.20
8.0–16.0 Å	0.20	–	0.16	0.28	0.12	0.12	0.16
Wyckoff site	*Occupation* (%)						
96*g*	29.6(2)	29.6	34.8(1)	29.2(2)	27.5(5)	29.9(2)	30.2(2)
32*e*	18.1(1)	18.1	11.3(2)	6.3(1)	17(1)	16.4(6)	15.6(1)
8*b*	0	0	2.6(2)	50(3)	27.3(4)	0	0

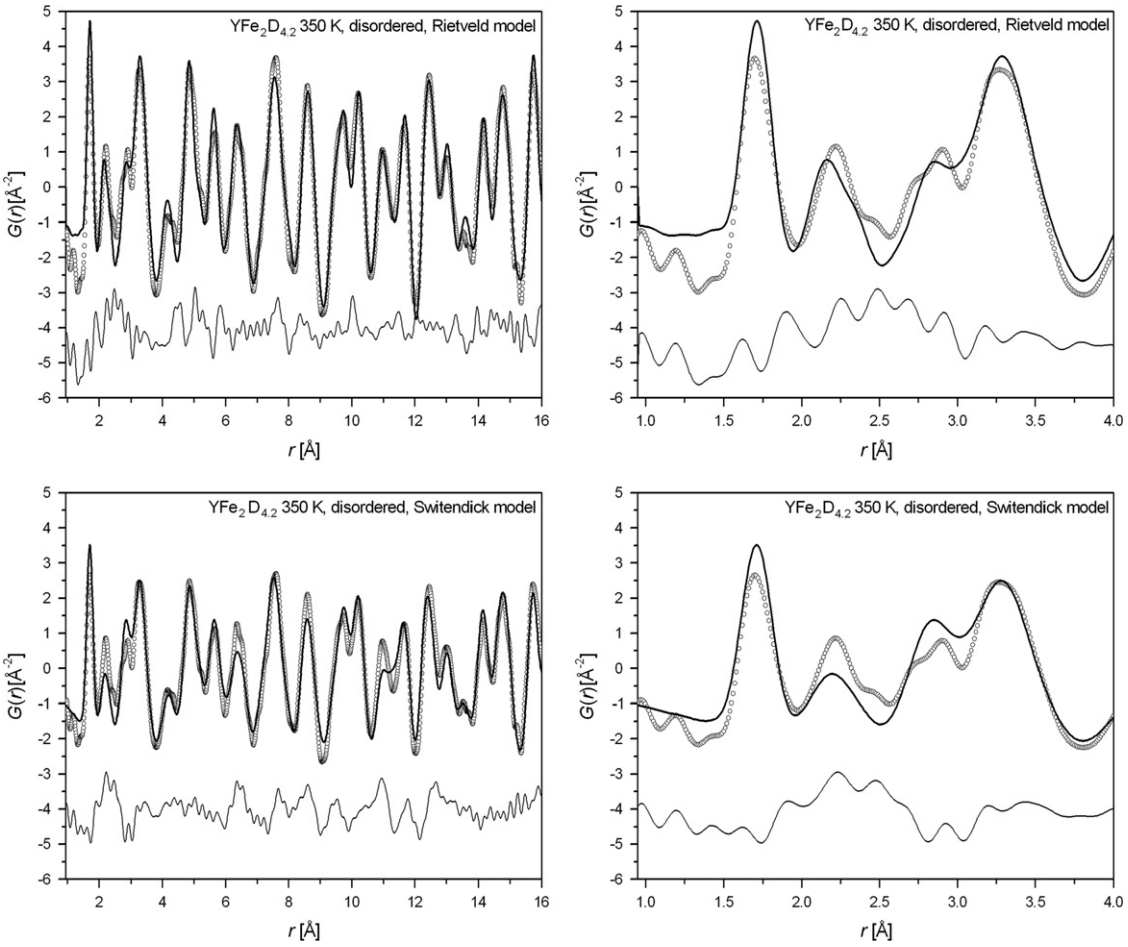

Fig. 6. Comparison of the observed PDF (points) with the calculated PDF (line) from the *Rietveld* refinement (top) of the HT-disordered $YFe_2D_{4.2}$ at 350 K, and from the *random* distribution of 34 deuterium atoms on 136 available positions (96*g*, 32*e*, 8*b*) with the only constrain of the minimal distance between two deuterium atoms of 1.96 Å (*Switendick model*, bottom).

significantly improved by the *long-range RMC model*. The reason for the latter is not clear. One possibility is that the *RMC modeling* without the *short-range* information simply over-fit the observed PDF. The deuterium distribution in the first coordination sphere of iron as produced by the *long-range RMC model* is not chemically sound, and contains many short D–D distances which are visible in the calculated PDF (Fig. 7 middle right). The *long-range RMC model* also produces a distribution of deuterium atoms between the three Wyckoff sites (96*g*, 32*e* and 8*b*) which is in strong disagreement with the distribution from *Rietveld model* especially on the 8*b* site. On the other side the distribution from the *short-range RMC model* is in good agreement with the *Rietveld model* and very close to the LT-ordered structure (Table 1). It clearly shows that the PDF in the range 0.95–3.8 Å contains important informations about the *short-range* ordering of deuterium atoms.

At first, in all RMC calculations, no constrain on the minimal D–D distance has been used, and the resulting models show very short D–D contacts. We have therefore combined the RMC modeling within the range 0.95–3.8 Å with the exclusion of the RMC moves leading to D–D distances shorter than 1.96 Å. Due to the calculation time limits a smaller refinement box of 8 Å size was used which is still twice of the modeled correlation distance. The resulting model, called *short-range RMC+Switendick model* is shown in Fig. 7 bottom and in Table 1. We can see that it explains the observed PDF up to 8 Å equally well as the *short-range model*, but without any short D–D contacts. As expected, above 8 Å, the agreement is worse, but comparable to the *Rietveld model*.

The similarity of both PDFs, LT-ordered and HT-disordered, below 8 Å has motivated us to construct the LT-ordered structure within one cubic unit cell of the HT-phase, and to calculate its PDF. The cells of the LT- and HT-phases contain the same number of atoms, but have different translation symmetry, therefore only the PDF up to $r \sim 8$ Å (one cubic cell) can be compared. Without a big surprise, the *LT-ordered model* fits also quite well the observed PDF of the HT-disordered phase up to $r \sim 8$ Å (Table 1 and Supporting Information, Fig. S5).

Finally neutron powder diffraction patterns were calculated from the *short-range RMC+Switendick model* to verify that the model explains well the observed diffuse intensity. A $15 \times 15 \times 15$ ($=3375$) super-cell was created from 8 unit cells of randomly selected optimizations. The total number of 3375 unit cells was obtained by applying randomly twelve point symmetry operations of the 1/2, 1/2, 1/2 point to the 8 unit cells. The neutron powder pattern was then calculated using the Debye formula option in the *DISCUS* program. The same procedure was used also to calculate the powder patterns of the *Rietveld* and *Switendick models*. The calculated neutron powder patterns are compared in Fig. 8 with the observed pattern from the medium resolution data bank of the GPPD diffractometer. As one can see the *short-range RMC+Switendick model* explains well the Bragg intensity and most of the observed diffuse intensity. On the other side the *Switendick model* shows the diffuse intensity in the correct *Q* interval but weaker than the observed diffuse intensity. Moreover, the *Switendick model* produces important changes in the Bragg intensities as it changes the distribution of deuterium atoms

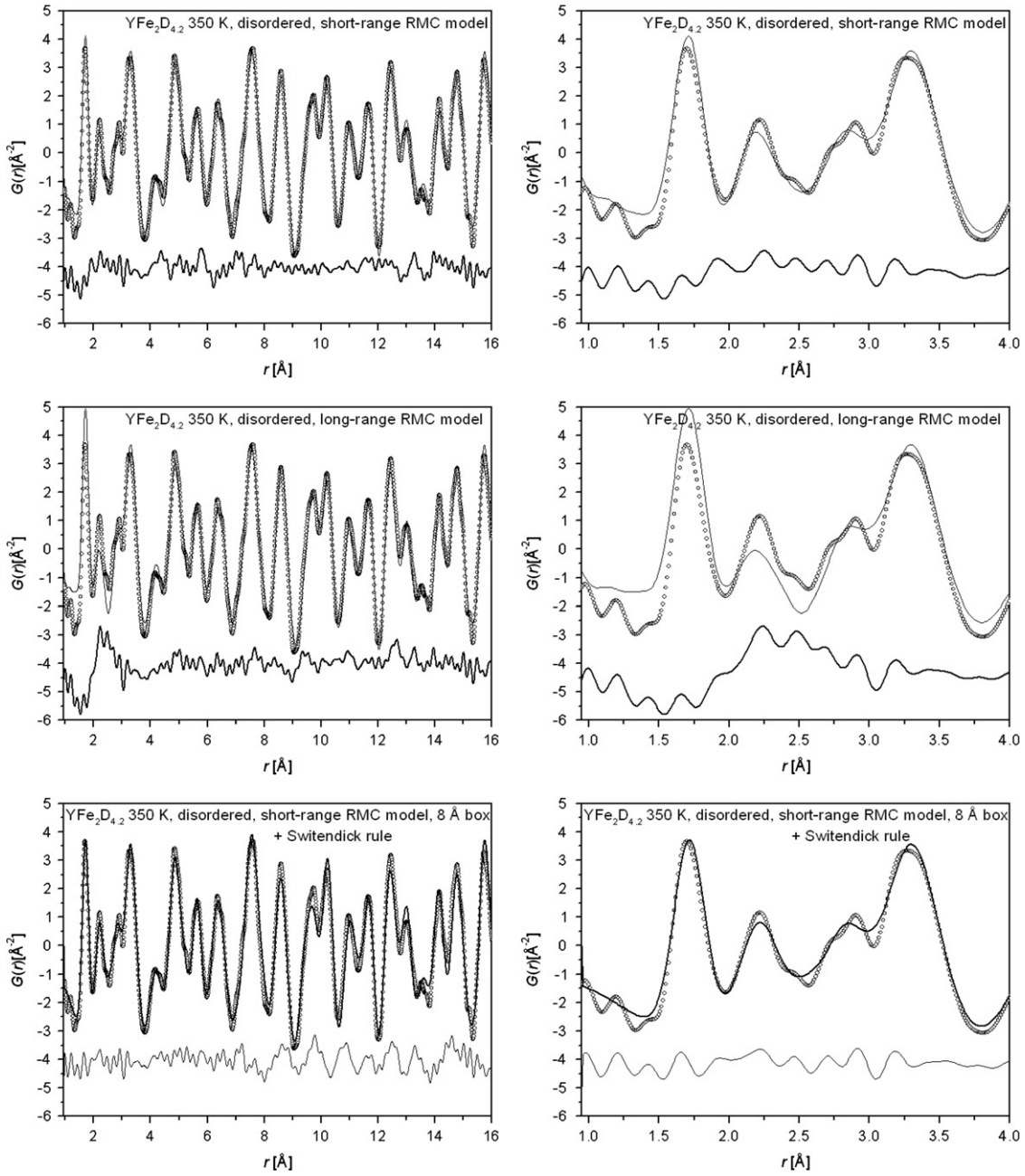

Fig. 7. Comparison of the observed PDF (points) with the calculated PDF (line) from the *RMC modeling* of the HT-disordered $YFe_2D_{4.2}$ at 350 K: modeling within the *r*-range 0.95–3.8 Å (*short-range RMC model*, top), and within the *r*-range 3.8–8.0 Å (*long-range RMC model*, middle). Combining the *short-range modeling* with the *Switendick rule* (*short-range RMC+Swidendick model*) within the 8 Å box is shown at the bottom.

between the sites 96*g*, 32*e* and 8*b* from the distribution observed in the *Rietveld model* and in the *short-range RMC model*. Finally the *Rietveld model*, as expected, produces no diffuse intensity.

3.5. Local deuterium order

A statistical analysis of the iron coordination by deuterium was done for all models and is shown in Fig. 9. The LT-ordered phase has only two types of coordination: 4- and 5-fold in the ratio 1/7. While the *long-range RMC modeling* converged to a broad distribution ranging from 1 to more than 8, the *short-range RMC modeling* clearly prefers 4- and 5-fold coordination as in the LT-ordered phase. The preference is even enhanced by the applications of the Switendick rule in the *short-range RMC+Swidendick model* resulting in the 4- and 5-fold coordination exclusively in the ratio 5/6.

The application of the Switendick rule itself is not enough to model the observed PDF in the range up to $r\sim3.8$ Å as already discussed. Especially the first two PDF peaks containing the correlations from the first coordination spheres Fe–D, D–D and Y–D are badly modeled in the *Switendick model*. It points out the presence of another correlation in addition to D–D repulsion. This correlation is probably the directional Fe–D bonding. As discussed already in Ref. [10] the FeD_5 and FeD_4 polyhedra in LT-ordered phase cannot be considered as anionic 18-electron complexes as observed in so-called "complex" transition metal hydrides. However, the directional *B*–D bonding cannot be neglected neither in the so-called "interstitial" metal hydrides like $YFe_2D_{4.2}$, and determines the coordination number and the shape of the BD_x

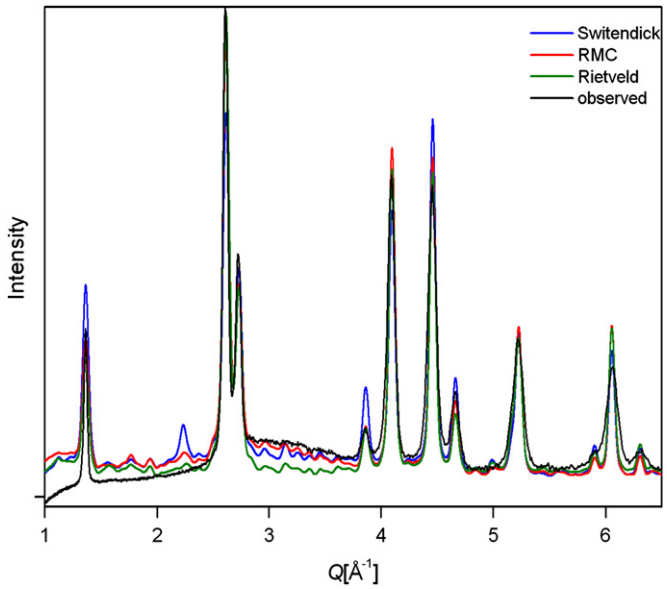

Fig. 8. Comparison of neutron powder patterns (normalized intensity *vs.* *Q*) from HT-disordered $YFe_2D_{4.2}$ phase (350 K): as observed from medium resolution GPPD data bank, and as calculated from the *Rietveld*, *Switendick* and *short-range RMC+Swidendick models*.

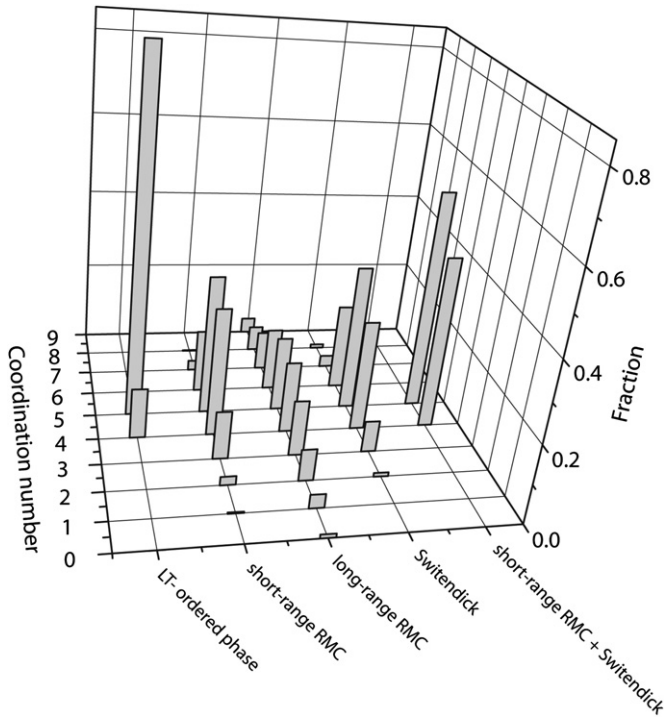

Fig. 9. Distribution of iron coordination by deuterium for different models of HT-disordered $YFe_2D_{4.2}$ at 350 K.

coordination polyhedron (see [30] for a similar discussion about deuterides of AB_3 compounds).

Concerning the shape of FeD_5 and FeD_4 polyhedra as obtained from the *short-range RMC+Switendick model*, the analysis has not provided any preference for a trigonal bi-pyramid or regular tetrahedron, as observed in the LT-ordered phase. Very distorted polyhedra have been mostly observed. However, the information about the direction of the Fe–D vectors is contained in the PDF only indirectly through the distribution of D–D distances, and we conclude that the exact shape of the FeD_x coordination polyhedra cannot be unambiguously revealed by the PDF analysis.

The analysis of different possibilities how to distribute D atoms in three interstitial sites (96*g*, 32*e* and 8*b*) of the cubic Laves phases AB_2 has been done in ref. [31]. The analysis has concentrated on the distribution of D atoms around the *A* atom, and it has been shown that it is possible to locate a maximum of 12D atoms around an *A* atom without creating short D–D contacts. This leads to a maximal deuterium content of 6 D/f.u. If the shifts of D atoms from the centers of the interstitial sites are allowed, then the maximal D content increases to 7 D/f.u.

We have analyzed the distribution of D atoms around the *B* atom (iron in our case) in the cubic Laves phases AB_2. Our preference for the *B*-coordination over the *A*-coordination is justified by the importance of Fe–D over Y–D bonding for stabilizing the monoclinic structure of the LT-ordered phase as shown in [32]. It is possible to distribute randomly up to 7 deuterium atoms in average around each iron without shifting the deuterium atoms from the average positions, and without any D–D distances below 1.96 Å. Half the Fe atoms will be coordinated by 8D (6 on 96*g* and 2 on 8*b*), and half by 6D (4 on 96*g* and 2 on 8*b*). This leads to the average D content of 6 D/f.u. If the 32*e* site is involved than a maximum of 6D atoms can be distributed, 4 in 96*g*, 1 in 32*e* and 1 in 8*b*. This leads to the deuterium content of $5\frac{1}{6}$ D/f.u. However, in the LT-ordered phase of $YFe_2D_{4.2}$ the 8*b* site is empty (notation of Wyckoff sites w.r.t. HT-disordered phase), 7Fe atoms are coordinated by 5D (4 on 96*g* and 1 on 32*e*), and Fe8 is coordinated by 4D (2 on 96*g* and 2 on 32*e*) leading to the maximal deuterium content of 4.5 D/f.u. The absence of 8*b* site in deuterium distribution is conserved also in the HT-disordered phase as observed from the *Rietveld refinement* [10] and from our *short-range RMC modeling* resulting in the preferred coordination of 5 and 4D atoms around each Fe. If the deuterium shifts were allowed then a maximal deuterium capacity of 6 D/f.u. could be obtained in the cubic lattice of the Laves phase keeping the 8*b* site empty as observed in ZrV_2D_6 [33]: 8 deuterium atoms around V1 (4 on 96*g* and 4 on 32*e*), and 7 around V2 (2 on 96*g* and 5 on 32*e*). Interestingly, when applying high deuterium pressure (~1 GPa) to YFe_2 it is possible to insert up to 5 D/f.u [6]. The YFe_2D_5 phase crystallizes in the orthorhombic structure with s.g. $Pmn2_1$ [8]. The metal atoms are shifted from the average positions of the cubic lattice, and the original cubic 8*b* site remains empty. Two of three Fe are coordinated by D in a trigonal bipyramid (with apical vertices disordered between two close 96*g* sites), and the third one by an octahedron.

3.6. PDF studies of SRO in metal hydrides—perspectives

In conclusion, we have successfully performed a study of the chemical SRO by applying the PDF analysis and using neutron (*ToF*) powder data. Such study was previously shown as feasible using simulated data of the metallic alloy Cu_3Au [34], and experimentally proved for the first time in Ref. [35].

The PDF investigation of the chemical SRO in metal hydrides (for review see [36]) was motivated by the wish to experimentally determine the H–H or D–D shortest distance in disordered systems. In the analysis of α-$VD_{0.8}$ [11] and $ZrCr_2D_4$ [15] the *RMC modeling* of the diffuse intensity in the neutron powder pattern (modeling in the reciprocal space) [19] was used due to the lack of high *Q*-data in the constant wavelength neutron data needed for the Fourier transformation to the PDF. In this work we have used the PDF analysis (modeling in the direct space) [19], since the high *Q*-data was available from the *ToF* neutron source. The advantage of the PDF method is that the experimentally derived PDF is an absolute function, and great-deal of structural information can be therefore deduced directly from the data without any modeling. We encourage therefore the use of *ToF* neutron scattering data whenever available.

4. Conclusions

The deuterium SRO in C-15 Laves phase deuteride $YFe_2D_{4.2}$ has been investigated by the neutron (*ToF*) powder diffraction experiments and Pair Distribution Function (PDF) analysis between 290 and 400 K. PDFs of HT-disordered (350 and 400 K) and LT-ordered phases (290 K) of $YFe_2D_{4.2}$ look similarly up to the distance of $r\sim3.8$ Å, which includes all interactions within the first coordination sphere around iron and yttrium atoms. The similarity of the observed PDFs can be understood as a similarity of the local structures of LT-ordered and HT-disordered phases up to the correlation length of $r\sim3.8$ Å, at least within the radial projection onto the PDF. In contrast to the SRO the LRO in both phases is quite different as it is reflected in the increased difference of PDFs above $r\sim8$ Å.

The minimal allowed D–D distance in a metal hydride of 2.1 Å (Switendick rule) has been observed and experimentally proved by the PDF analysis.

The PDF of HT-disordered $YFe_2D_{4.2}$ cannot be well explained in the range of interatomic distances which correspond to the first coordination spheres Fe–D, Y–D and D–D (up to $r\sim3.8$ Å) only by random occupation of available sites by deuterium atoms and application of the Switendick rule. On the other side it can be well explained by a SRO which, similarly to the LT-ordered phase, prefers 4- and 5-fold coordination of iron by deuterium. The exact shape of the coordination polyhedra cannot be unambiguously revealed by the PDF analysis.

The first PDF peak at $r\sim1.7$ Å corresponding to the first neighbor Fe–D distances is narrower than peaks at higher *r*-values showing so a correlated motion of FeD_5 and FeD_4 coordination polyhedra in both, LT-ordered and HT-disordered phases.

PDF modeling of neutron total scattering is a powerful tool for the analysis of metal-deuterium correlations in metal deuterides on different scales when completed by Bragg scattering analysis as done by the Rietveld method.

Acknowledgments

The authors thank to Thomas Proffen and Reinhard Neder for fruitful discussion about the analysis of disordered structures, and to Reinhard Neder also for the help with creating macros used by the program *DISCUS*. This work was supported by the Swiss National Science Foundation, Project no. 200021-107916.

Appendix A. Supplementary materials

Supplementary materials associated with this article can be found in the online version at doi:10.1016/j.jssc.2011.07.028.

References

[1] K.H.J. Buschow, A.M. Van Diepen, Solid State Commun. 19 (1) (1976) 79–81.
[2] V.V. Burnasheva, E.E. Fokina, S.L. Troitskaya, K.N. Semenenko, Russ. J. Inorg. Chem. 29 (6) (1984) 792–794.
[3] K. Kanematsu, J. Appl. Phys. 75 (10) (1994) 7105–7107.
[4] K. Kanematsu, N. Ohkubo, K. Itoh, S. Ban, T. Miyajima, Y. Yamaguchi, J. Phys. Soc. Jpn. 65 (4) (1996) 1072–1076.
[5] V. Paul-Boncour, L. Guénée, M. Latroche, A. Percheron-Guégan, B. Ouladdiaf, F. Bourée-Vigneron, J. Solid State Chem. 142 (1999) 120–129.
[6] V. Paul-Boncour, S.M. Filipek, A. Percheron-Guégan, I. Marchuk, J. Pielaszek, J. Alloys Compd. 317–318 (2001) 83–87.
[7] V. Paul-Boncour, G. André, F. Bourée, M. Guillot, G. Wiesinger, A. Percheron-Guégan, Physica B 350 (2004) e27–e30.
[8] G. Wiesinger, V. Paul-Boncour, S.M. Filipek, Ch. Reichl, I. Marchuk, A. Percheron-Guégan, J. Phys: Condens. Matter 17 (2005) 893–908.
[9] V. Paul-Boncour, M. Guillot, G. André, F. Bourée, G. Wiesinger, A. Percheron-Guégan, J. Alloys Compd. 404–406 (2005) 355–359.
[10] J. Ropka, R. Černý, V. Paul-Boncour, Th. Proffen, J. Solid State Chem. 182 (2009) 1907–1912.
[11] M.H. Sørby, A. Mellergård, R.G. Delaplane, A. Wannberg, B.C. Hauback, H. Fjellvåg, J. Alloys Compd. 363 (2004) 209–216.
[12] Bond, R.A., 1981. Ph.D. Thesis, University of Birmingham, England.
[13] A.V. Irodova, V.P. Glazkov, V.A. Somenkov, S. Shil'shtein, Fiz. Tverd. Tela 22 (1980) 79 (Translated in Sov. Phys. Solid State 22 (1980) 45–50).
[14] Bull D.J., 2001. Ph.D. Thesis, University of Salford, England.
[15] M.H. Sørby, A. Mellergård, B.C. Hauback, H. Fjellvåg, R. Delaplane, J. Alloys Compd. 457 (2008) 225–232.
[16] H.M. Rietveld, J. Appl. Cryst. 2 (1969) 65–71.
[17] T.R. Welberry, Diffuse X-Ray Scattering and Models of Disorder. IUCr. Monographs on Crystallography, Oxford University Press, 2004.
[18] P. Debye, H. Menke, Phys. Z. (1930) 797.
[19] T. Egami, S.J.L. Billinge., Underneath the Bragg-Peaks: Structural Analysis of Complex Materials, Pergamon Press, Oxford, 2003.
[20] T.E. Faber, J.M. Ziman, Philos. Mag. 11 (1965) 153–173.
[21] B.E. Warren, X-ray Diffraction, Addison-Wesley, Reading, 1969 (Reprinted (1990). New York: Dover).
[22] F. Zernicke, J.A. Prins, Zeit Phys. 41 (1927) 184.
[23] P.F. Peterson, M. Gutmann, Th. Proffen, S.J.L. Billinge, J. Appl. Cryst. 33 (2000) 1192.
[24] C.L. Farrow, P. Juháš, J.W. Liu, D. Bryndin, E.S. Božin, J. Bloch, Th. Proffen, S.J.L. Billinge, J. Phys.: Condens. Matter 19 (2007) 335219.
[25] I.-K. Jeong, R.H. Heffner, M.J. Graf, S.J.L. Billinge, Phys. Rev. B 67 (2003) 104301.
[26] X. Qiu, E.S. Božin, P. Juhas, T. Proffen, S.J.L. Billinge, Reciprocal-space instrumental effects on the real-space neutron atomic pair distribution function, J. Appl. Cryst. 37 (2004) 110–116.
[27] Th. Proffen, R.B. Neder, J. Appl. Cryst. 30 (1997) 171–175.
[28] T. Leblond, V. Paul-Boncour, F. Cuevas, O. Isnard, J.F. Fernández, Int. J. Hydrogen Energy 34 (2009) 2278–2287.
[29] A.C. Switendick, Z. Phys. Chem. Neue Folge 117 (1979) 89–112.
[30] Y.E. Filinchuk, K. Yvon, J. Solid State Chem. 179 (2006) 1041–1052.
[31] A.B. Riabov, V.A. Yartys, J. Alloys Compd. 330–332 (2002) 234–240.
[32] V. Paul-Boncour, S.F. Matar, Phys. Rev. B 70 (2004) 184435.
[33] A.N. Bogdanova, A.V. Irodova, G. Andre, F. Bouree, J. Alloys Compd. 356–357 (2003) 50–53.
[34] Th Proffen, Z. Kristallogr. 215 (2000) 661–668.
[35] Petkov V. Proffen Th., S.J.L. Billinge, T. Vogt, Z. Kristallogr. 217 (2002) 47–50.
[36] M.H. Sørby, Z. Kristallogr. 223 (2008) 617–627.